Available online at www.sciencedirect.com
ScienceDirect
Journal of Nuclear Materials 360 (2007) 159–169
journal of nuclear materials
www.elsevier.com/locate/jnucmat

Object kinetic Monte Carlo study of sink strengths

Lorenzo Malerba [a], Charlotte S. Becquart [b,*], Christophe Domain [c]

[a] SCK•CEN, Reactor Materials Research Unit, Boeretang 200, B-2400 Mol, Belgium
[b] LMPGM, UMR-CNRS 8517, Université de Lille I, 59655 Villeneuve D'Ascq, France
[c] EDF-R&D, Department MMC, Les Renardières, Moret-sur-Loing, France

Received 17 July 2006; accepted 2 October 2006

Abstract

The sink strength for three-dimensionally (3D) versus one-dimensionally (1D), or mixed 1D/3D, migrating defects in irradiated materials has attracted much attention in the recent past, because many experimental observations cannot be interpreted unless 1D or mixed 1D/3D migration patterns are assumed for self-interstitial atom clusters produced in cascades during irradiation. Analytical expressions for the sink strengths for defects migrating in 3D and also in 1D have been therefore developed and a 'master curve' approach has been proposed to describe the transition from purely 1D to purely 3D defect migration. Object kinetic Monte Carlo (OKMC) methods have subsequently been used to corroborate the theoretical expressions but, although good agreement was generally found, the ability of this technique to reach the 1D migration limit has been questioned, the limited size of the simulation box used in OKMC studies having been mainly blamed for the inadequacies of the model. In the present work, we explore the capability of OKMC to reproduce the sink strengths of spherical absorbers in a wide range of volume fractions, together with the sink strength of grain boundaries, for defects characterised by different migration dimensionality, from fully 3D to pure 1D. We show that this technique is not only capable of reproducing the theoretical expressions for the sink strengths in the whole range of conditions explored, but is also sensitive enough to reveal the necessity of correcting the theoretical expressions for large sink volume fractions. We thereby demonstrate that, in spite of the limited size of the OKMC simulation box, the method is suitable to describe the microstructure evolution of irradiated materials for any defect migration pattern, including fully 1D migrating defects, as well as to allow for the effect of extended microstructural features, much larger than the simulation box, such as grain boundaries.

PACS: 82.20.Wt; 81.05.Bx

1. Introduction

The kinetic Monte Carlo (KMC) method provides solutions to the master equations of a physical system whose evolution is governed by a known set of transition rates between possible states, by choosing randomly among various possible transitions and accepting them on the basis of appropriate probabilities [1]. When applied to study the evolution of systems of mobile species, such as atoms (atomistic KMC, AKMC) [2–4] or defects formed under irradiation (object KMC, OKMC) [5–7] it

* Corresponding author. Tel./fax: +33 3 20 43 49 44.
E-mail address: charlotte.becquart@univ-lille1.fr (C.S. Becquart).

0022-3115/$ - see front matter © 2006 Elsevier B.V. All rights reserved.
doi:10.1016/j.jnucmat.2006.10.002

has the advantage of going beyond the mean-field approximation, by explicitly and spontaneously taking into account spatial correlations between the elements of the physical system. As such, KMC methods are expected to implicitly reproduce, among other phenomena, the effect of sinks or traps for migrating species, characterised by a given geometry and spatial distribution, i.e. these methods are expected to provide spontaneously the sink strengths typically used in the rate theory to describe the interaction of migrating defects with the features characterising the microstructure of the material (e.g. voids, dislocations, grain boundaries,...) [8–11].

The sink strength of each type of microstructural feature, k^2, is proportional to the square of the inverse of the mean distance covered by the migrating species before interacting with it, in general by being absorbed or trapped. The sink strength is a priori a function not only of the type, shape, orientation, size and concentration of the sinks, as well as, in principle, of the features of the actual interaction, but also, and sometimes crucially, of the dimensionality of the motion of the affected migrating species. In particular, the sink strength for three-dimensionally (3D) versus one-dimensionally (1D), or mixed 1D/3D migrating defects has attracted a lot of attention in the past decade, as a consequence of the fact that a number of experimental observations concerning irradiated materials under cascade damage conditions cannot be interpreted unless 1D or mixed 1D/3D migration patterns are assumed for self-interstitial atom clusters [12–14], which are by now well known to be produced directly in displacement cascades [15–17]. These types of migration patterns have been amply confirmed by a number of molecular dynamics simulation studies in α-Fe and Cu [18,19]. Thus, analytical expressions for the sink strengths for defects migrating not only in 3D [11], but also in 1D [20], have been developed for use in rate equation models of microstructure evolution under irradiation [13,14]. In addition, a 'master curve' approach has been proposed to describe the transition of the sink strength from purely 1D to purely 3D defect migration, as a function of the frequency of change of 1D motion direction [21]. OKMC methods have subsequently been used to corroborate the theoretical expressions [22–24]. Although in general good agreement has been found between analytical theory and simulation, in the cited work it has been pointed out that the OKMC methods are only of limited applicability to verify sink strength values. More specifically, the ability of this technique to reach the sink strength 1D migration limit has been questioned [25,24] and also apparent discrepancies between theory and simulation in the case of 3D migrating defects have remained unexplained [22]. The necessarily limited size of the simulation box used in OKMC studies has been mainly blamed for these inadequacies.

In the present work, we explore the capability of the OKMC technique to reproduce the sink strengths of spherical, unsaturable absorbers in a large range of volume fractions, as well as the sink strength of grain boundaries, for defects characterised by a varying motion dimensionality, from the fully 3D limit to the pure 1D limit. We show that this technique is not only capable of reproducing the theoretical expressions for the sink strengths in the whole range of conditions explored, but is also sensitive enough to reveal the necessity of appropriately correcting the theoretical expressions for large sink volume fractions. We thereby demonstrate that, in spite of the limited size of the OKMC simulation box, the method is indeed suitable to solve the equations governing the microstructure evolution of irradiated materials for any defect migration pattern, including fully 1D migrating defects, as well as to allow for the effect of extended microstructural features, much larger than the simulation box, such as grain boundaries. In Section 2 the computational method is described in detail. In Section 3 our results are presented, distinguishing between the cases of spherical absorbers for 3D, 1D and mixed 1D/3D migrating defects and grain boundaries. In Section 4 the capability of the OKMC technique to reliably evaluate sink strengths is discussed in the light of present and previous work. The main conclusions are summarised in Section 5.

2. Computational method

The general features of the OKMC code used in the present work, LAKIMOCA, have been extensively described in a previous publication [7]. Briefly, the model treats radiation produced defects (vacancies, self-interstitials atoms – SIA – and clusters thereof) as objects with specific positions in a simulation box and with associated reaction volumes. Each object can migrate and participate in a series of predefined reactions. The probabilities for physical transition mechanisms, which are basically migration jumps and emission from larger defects or from traps, are calculated in terms of Arrhenius

frequencies for thermally activated events, $\Gamma_i = \nu_i \exp\left(\frac{E_{a,i}}{k_B T}\right)$, where ν_i is the attempt frequency (prefactor) for event i, $E_{a,i}$ is the corresponding activation energy, k_B is Boltzmann's constant and T is the absolute temperature. The Monte Carlo algorithm [26] is used to select at each step the event that is going to take place, based on the corresponding probabilities, by extracting random numbers. After a certain event is chosen, time is increased according to the residence time algorithm, $\Delta\tau = 1/\sum_{i=1}^{N_e^{th}} \Gamma_i + \sum_{j=1}^{N_e^{ext}} P_j$ [27], where P_j are the probabilities of external events, such as the appearance of a cascade or of isolated Frenkel pairs produced by impinging particles. The choice of this expression is in the long term equivalent to choosing $\Delta\tau' = -\ln R \cdot \Delta\tau$, where R is a random number between 0 and 1 [28]. In addition, the model includes non-thermally activated events, such as the annihilation of a defect after encountering either a defect of opposite nature (i.e. a SIA encountering a vacancy) or a sink, as well aggregation, either by adding a point-defect to a cluster or by forming a complex between a defect and a trap for it. These events occur only on the basis of geometrical considerations (overlap of reaction volumes) and do not participate in defining the progressing of time. The possibility of introducing different classes of immobile traps and sinks, characterised by specific geometrical shapes (spheres, infinite cylinders, surfaces,...) and suitable to mimic voids or other trapping nano-features, as well as dislocations and grain boundaries, is also implemented. The code is therefore equipped to mimic realistic microstructures and irradiation conditions.

In the present work, however, the model is used to explore only idealised situations, as was done by Heinisch and co-workers [22,24], where only one migrating defect at a time is present in the simulation box, in a microstructure defined by only one or at the most two classes of sinks of precise geometry. The trajectory of the defect is followed until it is absorbed by a sink and at that point a new defect of the same type is introduced in the simulation box. The sink strength is obtained in this way as

$$k^2 = \frac{2n}{d_j^2 \langle n_j \rangle}, \tag{1}$$

where $\langle n_j \rangle$ is the average number of jumps performed by the defects, introduced one by one in the box, before being annihilated at the sink; n is the dimensionality of the motion and d_j is the jump distance. Since the defects are assumed to migrate in a body centered cubic (bcc) lattice, $d_j = \sqrt{3}/2 a_0$, where a_0 is the lattice parameter (in practice, the value for α-Fe has been used, i.e. $a_0 = 0.287$ nm). Note that, following the rate theory, the choice of n is not necessarily related to the actual dimensionality of the motion of the concerned defect, but rather to the choice of using, in the rate equations, the 3D or the 1D diffusion coefficient (D_3 or D_1) in the term reproducing the rate of annihilation at sinks, Dck^2, where c is the defect concentration [12,14,20]. Since in the present work the whole range of motion dimensionality, from 3D to 1D, is explored, in order to highlight the transition we make the consistent choice of using in all cases the 3D diffusion coefficient, i.e. throughout the paper $n = 3$ (unless otherwise stated). The histories of at least 1000 defects have been tracked for each condition in order to obtain the average $\langle n_j \rangle$ that appears in Eq. (1) and in most cases (all cases concerning 3D migrating defects and many concerning 1D migrating defects) the number was as high as 10000, or even more. In addition, it was always verified that the value had actually converged, i.e. that the average did not change significantly by increasing the number of followed defect histories. If this did not happen, the simulation was rejected and repeated with a larger number of sampled defects.

The dimensionality of the motion of the simulated defects has been defined in two ways. One way consisted in deciding that the defect must change direction of motion after a fixed number of jumps n_j^0, i.e. after having travelled a mean length $l_{ch} = d_j \sqrt{n_j^0}$. If $n_j^0 = 1$ the migration is fully 3D; the larger n_j^0, the closer the path becomes to being 1D. This is roughly the same scheme as in [22,24]. The other way consists in assigning an energy of rotation, E_r, whereby the probability of changing direction of motion is expressed as $\exp(E_r/k_B T)$. With this definition, the change of direction is simply another possible stochastic event managed by the Monte Carlo algorithm. Thus, the number of jumps executed by the defect before changing direction is not always the same, but in average it leads to a characteristic average segment length, $l_{ch} = d_j \sqrt{\exp(E_r/k_B T)}$. $E_r = 0$ provides a fully 3D path, while at the chosen simulation temperature of 573 K, $E_r = 1$ eV is enough to have a fully 1D path. Intermediate values (0.3, 0.35, 0.4, 0.45, 0.6, 0.7 and 0.8 eV were considered) correspond to mixed 1D/3D migration. Between each re-orientation, the defect moves along a ⟨1 1 1⟩ direction.

Non-cubic boxes with periodic boundary conditions (PBC) have been used for all calculations. The use of non-cubic boxes was found instrumental in order to simulate correctly the 1D migrating defects, as discussed in Section 4.

In the case of the spherical absorbers, boxes of $300 \times 350 \times 400$ lattice parameters, equivalent to a volume of about $10^6\,\mathrm{nm}^3$ if the lattice parameter of α-Fe is adopted, were used. The absorbers were randomly distributed in the simulation box, but care was taken to avoid overlap, in order to respect the assumptions made concerning their geometry, size and density. Their radius, R, was varied from 0.75 to 10.2 nm and their number density, N, from 10^{16} to $1.5 \times 10^{17}\,\mathrm{cm}^{-3}$, thereby spanning volume fractions, f_V, from 1.8×10^{-5} to 4.1×10^{-1}. The defects were introduced one by one in randomly selected positions within the simulation volume and the cases corresponding to defects created inside the absorbers were automatically excluded from the calculation of the average in Eq. (1).

The effect of the presence of spherical grain boundaries was introduced by assigning to each defect two positions: the relative position inside the simulation box, $\boldsymbol{s}$, and the absolute position inside the grain, $\boldsymbol{S}$. Two close-by defects in the simulation box will have similar relative positions, $\boldsymbol{s}_1$ and $\boldsymbol{s}_2$, but may have a priori completely different absolute positions in the grain, $\boldsymbol{S}_1$ and $\boldsymbol{S}_2$. Each time the defect crosses the box boundaries and PBC are applied to its relative position, $\boldsymbol{S}$ is corrected in such a way that the displacement of the defect to the image box beside is accounted for. If $\boldsymbol{S}$ gets to lie on the surface of the spherical grain, the defect disappears. In this scheme, the box size is totally decoupled from the grain size and the effect of the presence of large (spherical) grains can be allowed for, even using small simulation boxes. In the present case, boxes of $80 \times 120 \times 150$ lattice parameters ($3.4 \times 10^3\,\mathrm{nm}^3$) have been used and the grain size has been increased from 30 nm (the radius of the sphere enclosing the simulation box) to 1 μm and beyond, in some cases also with the addition of spherical absorbers in it.

3. Results

3.1. Spherical absorbers

According to theory, the sink strength of unsaturable spherical absorbers of radius R and density N for 3D migrating defects, $k^2_{3,\mathrm{s.a.}}$, can be expressed using the following, recursive expression (in defect of a bias factor) [8,11]:

$$k^2_{3,\mathrm{s.a.}} = 4\pi NR\left(1 + R\sqrt{k^2_{3,\mathrm{s.a.}}}\right). \tag{2}$$

This expression is, however, customarily truncated at the first order, $k^2_{3,\mathrm{s.a.}} = 4\pi NR$. In the case of 1D migrating defects, the expression for the sink strength, $k^2_{1,\mathrm{s.a.}}$, is exact and is given by [20]

$$k^2_{1,\mathrm{s.a.}} = 6(\pi R^2 N)^2. \tag{3}$$

(Always with the convention of using the 3D diffusion coefficient, D_3, in the equations, which explains the factor $6 = 3 \times 2$ in front of the parenthesis.) Given a defect that migrates following a path not coinciding with either the 3D or the 1D limit, the corresponding sink strength of spherical absorbers, $k^2_{1\text{–}3,\mathrm{s.a.}}$, can be expressed as a function of the two limiting case sink strengths and of the typical length for change of direction, l_{ch} [21]. After defining two dimensionless variables:

$$x^2 = \frac{l^2_{\mathrm{ch}} k^2_{1,\mathrm{s.a.}}}{12} + \frac{k^4_{1,\mathrm{s.a.}}}{k^4_{3,\mathrm{s.a.}}} \tag{4a}$$

and

$$y = \frac{k^2_{1\text{–}3,\mathrm{s.a.}}}{k^2_{1,\mathrm{s.a.}}}, \tag{4b}$$

the master curve relating the general case to the limiting cases is

$$y = \frac{1}{2}\left[1 + \sqrt{\left(1 + \frac{4}{x^2}\right)}\right]. \tag{4c}$$

These expressions will be used to benchmark the results of the simulation presented in the following subsections. Throughout the section, the results for the sink strengths will be represented in the figures as functions of the absorbers' volume fraction, f_V.

3.1.1. 3D migrating defects

Fig. 1 shows the cloud of simulation data points in two different ways. In the upper panel the data are grouped by absorber radii: points denoted by the same symbol correspond to the same absorber radius for growing absorber densities (1.0, 3.0, 6.0, 9.0, 12.0 and $15.0 \times 10^{16}\,\mathrm{cm}^{-3}$, the two highest densities were not considered in the case of the largest radius, though). In the lower panel, the simulation data are compared to the values obtained using

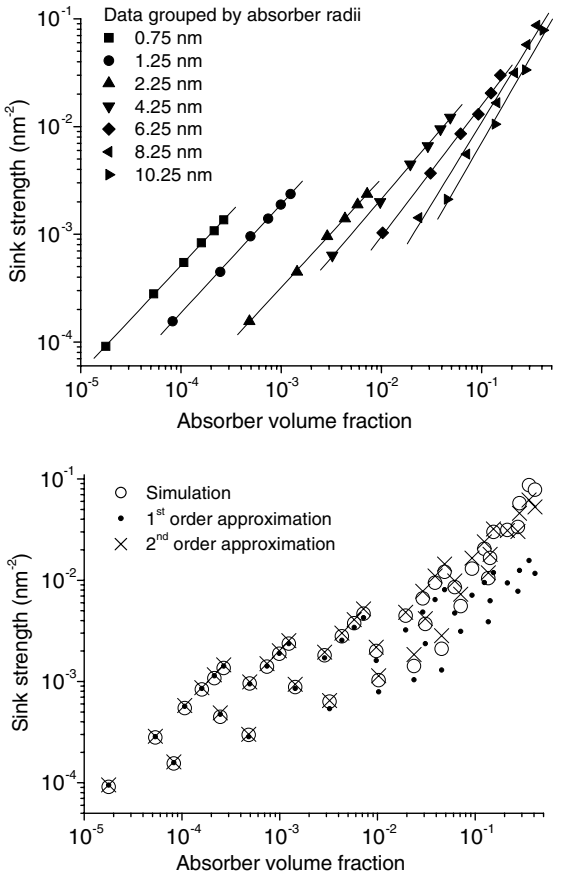

Fig. 1. Cloud of simulation data points for the sink strength of 3D migrating defects versus spherical absorber volume fraction. Above: grouped by absorber radii (the lines are simply guides for the eyes). Below: comparison with analytical expression (Eq. (2)) to first and second order.

the first order approximation expression for the sink strength from Eq. (2), $k^2_{3,\mathrm{s.a.}} = 4\pi NR$, denoted by small black dots, and also the second order approximation, $k^2_{3,\mathrm{s.a.}} = 4\pi NR(1 + R\sqrt{4\pi NR})$, indicated by crosses. Despite a small scatter on the data of Fig. 1, due to statistical fluctuations, it appears clearly that, in order for an agreement to be found between simulation and theory for volume fractions above 10^{-3} it becomes necessary to use the second order approximation of the formula, as the first order approximation largely underestimates the actual sink strength. Above $f_V = 10^{-1}$ even the second order approximation becomes insufficient and more terms should probably be recursively added. Fig. 2 suggests in a fairly clear way that this is indeed the case: the relative error, defined as percentage ratio of the difference between simulation and theory versus theory, using the second order

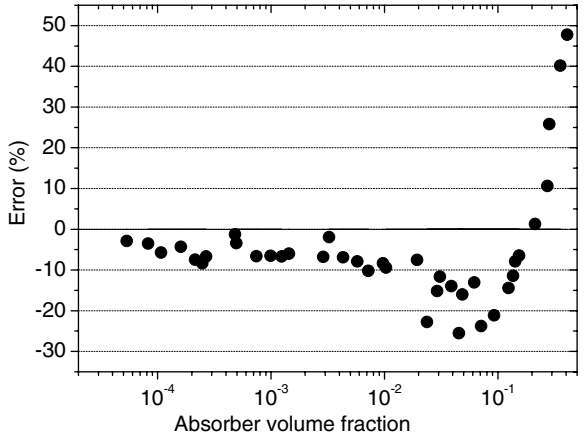

Fig. 2. Percentage error committed by using the simulation for 3D migrating defects results instead of the theoretical expression given in Eq. (2), in its second order approximation, versus spherical absorber volume fraction.

approximation as reference value, remains low in absolute value and negative in sign for low f_V, starts growing in absolute value above $f_V = 10^{-2}$ and above $f_V = 10^{-1}$ it even changes sign, becomes positive and grows very rapidly. The latter is clearly the consequence of the need for an additional correction in order to obtain agreement between theory and simulation data.

3.1.2. 1D migrating defects

Fig. 3 is the equivalent of Fig. 1 for 1D migrating defects. In the upper panel the simulation data points grouped by absorber radii are shown; in the lower one the same points are compared with the result of using Eq. (3). The equation is used to extend the data points to the whole range of volume fractions that was explored in the 3D case. As a matter of fact, it is impossible to produce statistically reliable results for 1D migrating defects when only very few small absorbers are present, for computing time reasons. Even after more than 10^{12} Monte Carlo time steps (corresponding to months of calculations on the used cluster of PCs), for volume fractions less than 10^{-3} the number of followed defect histories remained below 1000 and the sink strength value could be hardly said to have converged.

This is a direct consequence of the quadratic dependence of $k^2_{1,\mathrm{s.a.}}$ on the NR^2 product (Eq. (3)), to be compared with the 1st approximation linear dependence on NR in the 3D case (Eq. (1)), which makes the probability for the defect to encounter absorbers along its 1D path negligibly small for

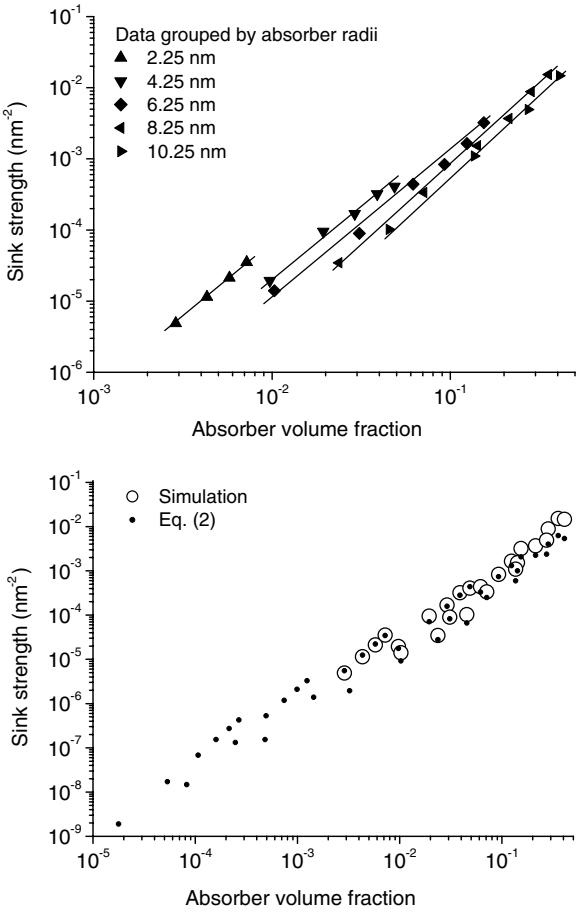

Fig. 3. Cloud of simulation data points for the sink strength of 1D migrating defects versus spherical absorber volume fraction. Above: grouped by absorber radii (the lines are simply guides for the eyes). Below: comparison with analytical expression (Eq. (3)). The theoretical points are extended to the same range of volume fractions as studied in the 3D case.

small values of NR, compared to a 3D migrating defect, as is also intuitive to imagine. By comparing the lower panel of Fig. 3 with the corresponding panel in Fig. 1 it can be seen that, for the same small volume fraction ($\sim 10^{-5}$), the absorber sink strengths for 3D migrating defects remains close to 10^{-4}, while it drops to 10^{-9} in the 1D case! The unlikelihood of encountering sinks along their path is, on the other hand, exactly the distinctive feature of 1D migrating defects, which defines their specificity and allows, trough the postulation of their existence, a number of experimental facts concerning microstructure evolution under irradiation to be understood [12,14].

This is also the reason why in general, and not only for small volume fractions, it is more difficult to obtain, by simulation of 1D migrating defects, sink strength results that converge to an average within a narrow enough range of fluctuations. This explains why the simulation data points in Fig. 3 are more scattered and less precise than in the 3D case. Fig. 4 shows the 'correction' factor that should be applied to the theoretical values from Eq. (3) in order to provide the same value as the simulation. This factor lies between 1 and 1.5 in most cases, i.e. the simulation tends to overestimate the sink strength value. This is the consequence of the fact that, unless an unachievably large amount of defect histories is followed, the statistics is always biased towards higher sink strengths, since in the limited time available to the simulation, if convergence is reached, histories that ended with an early annihilation in a sink will remain more likely to be sampled than histories leading to late annihilation; so the average will tend to be larger rather than smaller than the theoretical value. Nonetheless, the overall agreement is satisfactory, except for $f_V > 10^{-1}$, where an increase of this correction factor is registered. Since, however, the increase of the volume fraction is expected to improve, rather than worsen, the statistical significance of the sampling done in the simulation, the rapid increase of the correction factor for large volume fractions cannot be ascribed to lack of convergence. Two possible explanations can be put forward. One is that, similarly to the 3D case, for large volume fractions Eq. (3) ceases to be valid and corrections to it should be added. The other is that the use of periodic boundary conditions, in the case of many and large absorbers,

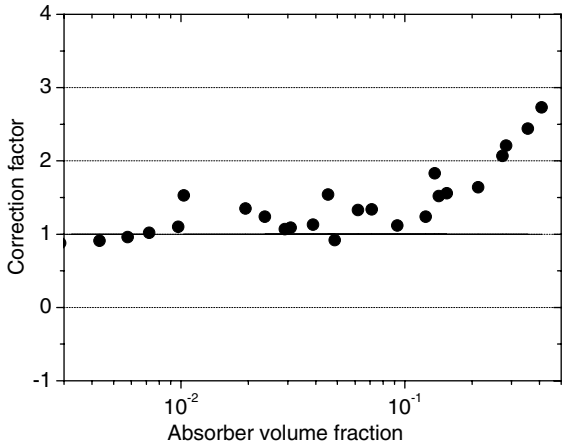

Fig. 4. Correction factor to be applied to Eq. (3) in order for it to coincide with the simulation results for 1D migrating defects, versus spherical absorber volume fraction.

introduces a certain degree of order in the simulation, which determines a departure from the theoretical expression, which is valid for randomly distributed sinks.

3.1.3. Transition between 3D and 1D regime

In Fig. 5, the simulated sink strength of different densities of spherical absorbers for defects that change ⟨1 1 1⟩ direction after a fixed amount of jumps, n_j^0, is plotted versus l_{ch}, which is made to vary between 1 and 100 000 nm. The absorber radius was 6.25 nm in all cases. In the same figure also the corresponding theoretical and simulation points for the purely 1D case are shown for comparison. This figure, which exemplifies the transition from 3D to 1D regime, should be compared with Fig. 2 in [24]. It can be seen that, differently from the figure in the cited work, in the present case the 1D limit was reached to very good approximation for $l_{ch} = 10$ μm and larger.

The same type of information, but in the master curve representation [21], is given in Fig. 6, where not only the points obtained from the simulations at fixed number of jumps used in Fig. 5 are included, but also those coming from simulations where the change of ⟨1 1 1⟩ direction was decided based on an energy of re-orientation, E_r. In the latter case, groups of points characterised by the same E_r (and therefore by the same l_{ch}) correspond to different densities and radii, in the range specified above for 1D simulations. It is noteworthy that all points fulfil the condition embodied by the master curve, with very little scatter only in the region of the transition (change of slope of the curve) and then, as expected, in the 1D region (where the curve remains constant). This indirectly suggests that it is irrelevant, in practice, how the change of direction is imposed.

3.2. Grain boundaries

According to theory, the sink strength of a spherical grain boundary of radius R_g for 3D migrating defects, $k^2_{3,g.b.}$, is [10]

$$k^2_{3,g.b.} = 14.4/R_g^2. \tag{5}$$

In the case of 1D migrating defects, the expression for the sink strength, $k^2_{1,g.b.}$, is also very similar [29]:

$$k^2_{1,g.b.} = 15/R_g^2. \tag{6}$$

(With the convention of using the 3D diffusion coefficient, D_3, in the equations.) If other sinks are present in the bulk, with sink strength $k^2_{s.b.}$, the sink strength of the grain boundary will be affected and can be expressed, through the dimensionless variables

$$\alpha = k_{s.b.}R_g \tag{7a}$$

and

$$\gamma = k^2_{g.b.}R_g^2, \tag{7b}$$

as

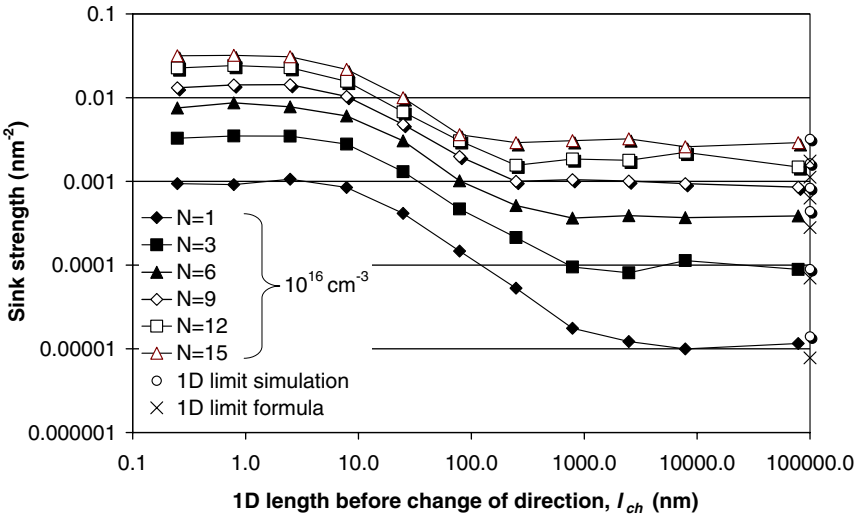

Fig. 5. Transition from 3D to 1D sink strength for different spherical absorber densities, as a function of the length of the 1D segments composing the 1D/3D migration path, $l_{ch} = d_j\sqrt{n_j^0}$, where d_j is the jump distance and n_j^0 the fixed number of jumps before changing direction. The corresponding 1D limit values from the simulation and from Eq. (3) are also indicated.

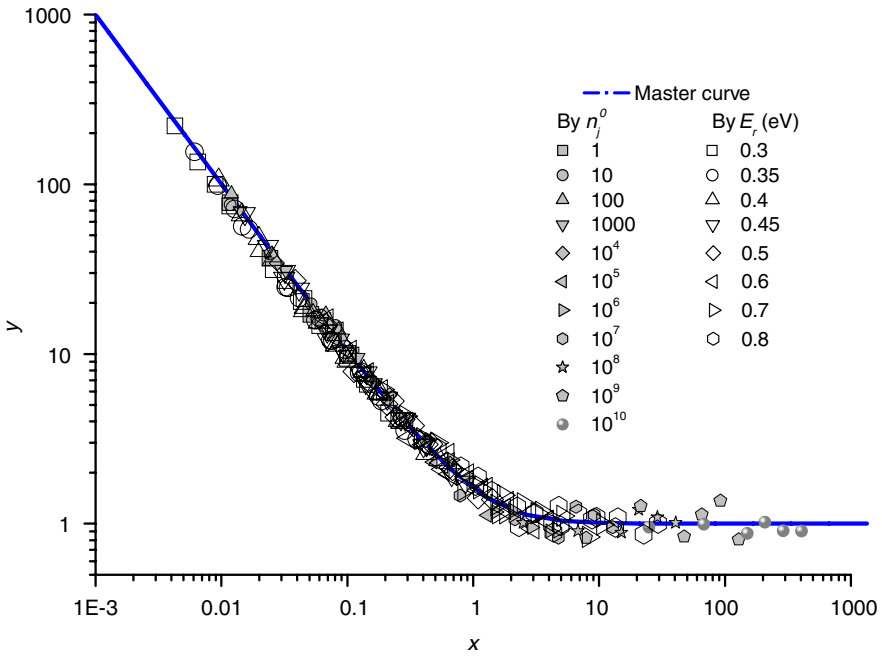

Fig. 6. Master curve representation of the transition from 3D to 1D regime in the case of the sink strength of spherical absorbers. The curve corresponds to Eq. (4c). The points are the result of obtaining x and y by applying Eqs. (4a) and (4b), using sink strength values for the 3D and 1D limit, as well as for the mixed 1D/3D case, taken from the simulation. The data points are grouped according to the criterion used to decide the change of direction, fixed number of jumps, n_j^0, or energy of rotation, E_r (see text). Each group of points spans a range of absorber radii and densities.

$$\gamma = \frac{3}{2}\left\langle 3+4\beta-\frac{6\beta(\beta-1)}{\alpha^2}+\left\{\left[3+4\beta-\frac{6\beta(\beta-1)}{\alpha^2}\right]^2 -4(\beta^2-\alpha^2)\left[2-\frac{3(\beta-1)}{\alpha^2}\right]^2\right\}^{1/2}\right\rangle \Big/ \left[2-\frac{3(\beta-1)}{\alpha^2}\right]^2, \tag{7c}$$

where $\beta = \alpha\coth\alpha$. This is a kind of 'master curve' for the grain boundary sink strength, explicitly derived in the case of 3D migrating defect (we are not aware of any specific derivation of this curve for 1D migrating defects). These expressions will

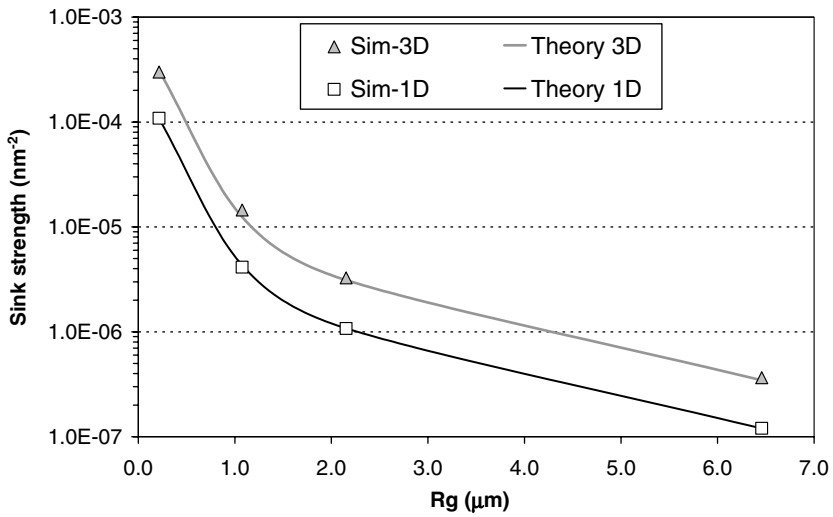

Fig. 7. Sink strength of a spherical grain boundary as a function of its radius for both 3D and 1D migrating defects. Lines corresponds to theoretical expressions, dots correspond to simulation results. The 1D data have been divided by three for better legibility of the figure, otherwise the two curves and dot series would have appeared superposed.

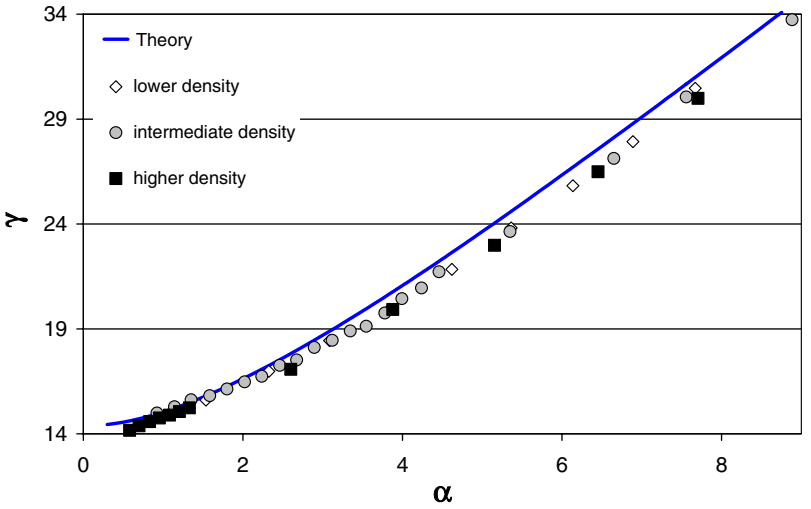

Fig. 8. Relationship between the sink strength of a spherical grain boundary and the sink strength of bulk sinks in terms of the dimensionless variables and master curve given in Eqs. (7). Three different spherical absorber densities (2.94, 5.88 and 8.81×10^{17} cm^{-3}) and a range of grain boundary radii (30 nm to 1 μm) have been considered.

be used to benchmark the results of the simulation presented in what follows.

Fig. 7 shows the sink strength of a spherical grain boundary as a function of its radius. The curves correspond to Eqs. (5) and (6), while the dots are the results of the OKMC simulation. For better legibility, in this figure the curve and dots for the 1D limit have been divided by three (thereby implying the use of a 1D diffusion coefficient, D_1, in the corresponding rate equations). The agreement between simulation and theory is self-evident.

The effect of the simultaneous presence of bulk sinks and grain boundaries has been explored by considering three densities of 3 nm radius absorbers, namely 2.94, 5.88 and 8.81×10^{17} cm^{-3}. 3D migrating defects have been introduced one by one and the grain boundary radius has been made to vary between 30 nm and 1 μm. The simulation results are plotted in Fig. 8 in terms of the dimensionless variables defined in (7a) and (7b) and compared with the 'master curve' given by Eq. (7c). Although the simulation results systematically lie slightly below the theoretical curve, the agreement is nevertheless remarkable.

4. Discussion

The results we have presented lead to a series of important statements. First, the OKMC technique, in spite of its inherently stochastic and discrete nature, can trustfully describe the strength of sinks of given geometry, size and density in a large range of sink volume fractions, in full agreement with theoretical expressions obtained in the framework of a mean-field, continuum approach. Second, in spite of the finiteness and relatively small size of the simulation box, this technique is capable of treating in a reasonably correct way also 1D migrating defects, whose path is orders of magnitude longer than the typical size of the box (provided that a non-cubic box is used, as will be shortly discussed). Third, also extended sinks much larger than the size of the OKMC simulation box can be correctly described by this technique. None of these statements could be obviously deduced from the existing literature on the subject.

In [22], the sink strength of spherical absorbers of growing radius for 3D migrating defects was found to diverge from the linear behaviour provided by the first order approximation of Eq. (2), and the authors fitted their results to a third degree polynomial. However no clear reason was provided for this discrepancy. We have shown that both our simulation results and those in [22] are consistent with the theoretical expression, provided that the latter is extended to further orders of approximation.

In [25], the conclusion of a kinetic Monte Carlo study of damage accumulation in metals under cascade irradiation conditions was that the applicability of such a technique was limited to cases where 1D diffusing defects have no consequential role on the microstructure evolution. Such a conclusion was

reached on the basis of the fact that the application of PBC seemed to produce a situation where the length of the path of 1D diffusing defects was not limited by the distance between sinks, but rather by events such as recombinations, which are the more frequent, the higher the dose; different results were obtained when applying a mean-field approach. On the other hand, the application of pseudo-periodic boundary conditions was shown to inherently destroy the one-dimensionality of the motion and was therefore rejected as a solution. In the course of the present work we have clearly observed that, if a cubic box is used, only two situations can be encountered in the case of 1D migrating defects with PBC: either no sink is located along their path, so that the defect can only indefinitely cross the simulation box without ever being absorbed; or a sink is indeed located along the path of the defect, but in this case the length travelled by the migrating object can only be of the order of the size of the box. In these conditions, the correct simulation of the absorption of 1D migrating defects is indeed unfeasible. If, on the other hand, non-cubic (i.e. parallelepipedic) boxes are used, then the application of PBC naturally provides the possibility for the defect to travel long distances without being absorbed in a sink and, conversely, of finding at some point a sink that can absorb it, even without changing direction of motion. This is illustrated pictorially in Fig. 9 and essentially happens because not only these defects move in 1D, but the possible direction of motion, $\langle 1\,1\,1\rangle$, is dictated by the crystallography and does not change if the box shape changes. Non-cubic boxes allow the defect to explore most of the box, by repeatedly applying PBCs, thereby changing the local landscape seen by the defect, although of course in the long run a certain degree of periodicity will appear. More generally, the key point is to have boxes that change dimension in directions that are not parallel to the fixed 1D motion direction. In [25], cubic boxes were used and we believe that this may have been the origin of the discrepancies from the mean-field approach found in that work. It remains nonetheless true that the OKMC simulation of 1D migrating defects requires, in order to be reliable, very long computing time, so as to produce a statistically representative sample of defect histories. To this regard, a point that remain to be clarified is the growing discrepancy between theory and simulation in the case of 1D migrating defects for large sink volume fractions, which may be due to the fast establishment of a certain periodicity and therefore order or simply to the inadequacy

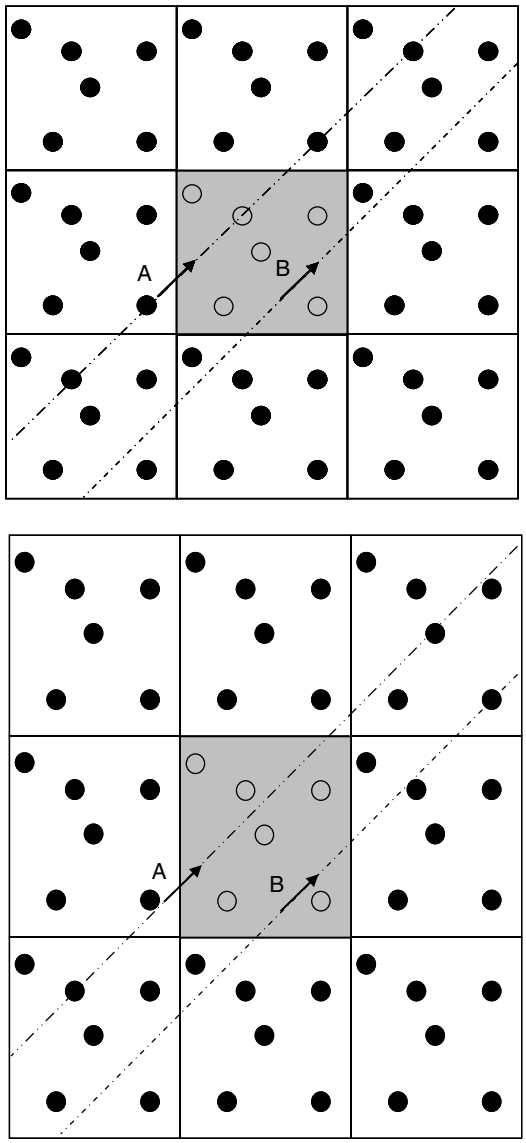

Fig. 9. Pictorial explanation (in 2D) of why the use of non-cubic boxes with PBC allows the simulation of 1D migration paths of a priori any length, while cubic boxes with PBC lead to unrealistic situations (the grey one is the simulation box, the others are the image boxes according to PBC). Above, path A is doomed to see the defect migrating along it to be immediately absorbed by the sink located on it, while along path B the defect can migrate indefinitely without ever encountering a sink. Below, because the migration direction remains unchanged, by stretching the same box to a non-cubic shape it becomes possible for the defect to migrate through many image boxes before being absorbed by a sink.

of the theoretical expression in that range of volume fractions.

Finally, in the present work we have shown that by assigning parallel coordinates to defects, i.e.

absolute coordinates inside a grain and relative coordinates inside the simulation box, the effect of extended defects such as grain boundaries can be allowed for even with a relatively small simulation box. The same approach can in principle be applied for other types of extended defects, a priori also with non-spherical shapes.

5. Conclusions

We have demonstrated that the OKMC technique naturally lends itself for the simulation of processes leading to radiation produced defect absorption at sinks, in the whole range of defect migration patterns, from fully 3D to purely 1D, and including the case of extended sinks much larger than the simulation box itself. In the present work we have dealt with sinks characterised by a well defined geometry and for which analytical expressions exist, so as to be able to prove the capability of the simulation model to provide correct results by comparison with those expressions. It is however believed that this simulation technique is suitable to provide correct results for, a priori, any sink type, shape and orientation, as well as in a large range of sink volume fractions, thereby going beyond the possibilities of mean-field theoretical approaches. The main exception is given by those cases where the sink volume fraction is very small, in which the production of statistically meaningful samples of defect histories may be difficult to achieve. In those cases only analytical expressions become applicable in practice.

Acknowledgements

This work was performed in the framework of the Perfect IP, partially funded by the European Commission within the 6th Framework Programme (contract no. FI6O-CT-2003-508840). The assistance of H. Trinkaus with the intricacies of the rate theory is gratefully acknowledged. The three authors wish also to thank S. Golubov for very useful discussions.

References

[1] K.A. Fichthorn, W.H. Weinberg, J. Chem. Phys. 95 (2) (1991) 1090.
[2] C. Domain, C.S. Becquart, J.C. van Duysen, Mater. Res. Soc. Symp. Proc. 540 (1999) 643.
[3] C. Domain, C.S. Becquart, J.C. van Duysen, Mater. Res. Soc. Symp. Proc. 650 (2001) R3.25.1.
[4] F. Soisson, J. Nucl. Mater. 349 (3) (2006) 235.
[5] M.J. Caturla, N. Soneda, E. Alonso, B.D. Wirth, T. Díaz de la Rubia, J.M. Perlado, J. Nucl. Mater. 276 (2000) 13.
[6] N. Soneda, S. Ishino, A. Takahasi, K. Dohi, J. Nucl. Mater. 323 (2003) 169.
[7] C. Domain, C.S. Becquart, L. Malerba, J. Nucl. Mater. 335 (2004) 121.
[8] A.D. Brailsford, J.R. Matthews, R. Bullough, J. Nucl. Mater. 79 (1979) 1.
[9] R. Bullough, M.R. Hayns, C.H. Woo, J. Nucl. Mater. 84 (1979) 93.
[10] R. Bullough, M.R. Hayns, M.H. Wood, J. Nucl. Mater. 90 (1980) 44.
[11] A.D. Brailsford, R. Bullough, Philos. Trans. R. Soc. London 302 (1981) 87, and references therein.
[12] H. Trinkaus, B.N. Singh, A.J.E. Foreman, J. Nucl. Mater. 199 (1992) 1;
H. Trinkaus, B.N. Singh, A.J.E. Foreman, J. Nucl. Mater. 206 (1993) 200;
H. Trinkaus, B.N. Singh, A.J.E. Foreman, J. Nucl. Mater. 249 (1997) 91;
H. Trinkaus, B.N. Singh, A.J.E. Foreman, J. Nucl. Mater. 251 (1997) 172.
[13] S.I. Golubov, B.N. Singh, H. Trinkaus, J. Nucl. Mater. 276 (2000) 78.
[14] H. Trinkaus, B.N. Singh, S.I. Golubov, J. Nucl. Mater. 283–287 (2000) 89.
[15] T. Diaz de la Rubia, R.S. Averback, H. Hsieh, R. Benedek, J. Mater. Res. 4 (1989) 579.
[16] A.F. Calder, D.J. Bacon, J. Nucl. Mater. 207 (1993) 25.
[17] W.J. Phythian, R.E. Stoller, A.J.E. Foreman, A.F. Calder, D.J. Bacon, J. Nucl. Mater. 223 (1995) 245.
[18] Yu.N. Osetsky, D.J. Bacon, A. Serra, B.N. Singh, S.I. Golubov, J. Nucl. Mater. 276 (2000) 65.
[19] Yu.N. Osetsky, D.J. Bacon, A. Serra, B.N. Singh, S.I. Golubov, Philos. Mag. 83 (2003) 61.
[20] A.V. Barashev, S.I. Golubov, H. Trinkaus, Philos. Mag. A 81 (10) (2001) 2515.
[21] H. Trinkaus, H.L. Heinisch, A.V. Barashev, S.I. Golubov, B.N. Singh, Phys. Rev. B 66 (2002) 060105(R).
[22] H.L. Heinisch, B.N. Singh, S.I. Golubov, J. Nucl. Mater. 283–287 (2000) 737.
[23] H.L. Heinisch, B.N. Singh, J. Nucl. Mater. 307–311 (2002) 876.
[24] H.L. Heinisch, B.N. Singh, Philos. Mag. 83 (31–34) (2003) 3661.
[25] A.V. Barashev, D.J. Bacon, S.I. Golubov, J. Nucl. Mater. 276 (2000) 243.
[26] N. Metropolis, A.W. Rosenbluth, M.N. Rosenbluth, A.H. Teller, E. Teller, J. Chem. Phys. 21 (1953) 1087.
[27] W.M. Young, E.W. Elcock, Proc. Phys. Soc. 89 (1966) 735.
[28] B. Bortz, M.H. Kalos, J.L. Lebowitz, J. Comp. Phys. 17 (1) (1975) 10.
[29] A.V. Barashev, Private communication.